NOTES AND CORRESPONDENCE

An Improved Moment Conservation Method for the Advection–Diffusion Equation

R. I. SYKES AND D. S. HENN

ARAP Group, California Research and Technology Division, Titan Corporation, Princeton, New Jersey

11 February 1991 and 30 May 1991

1. Introduction

Numerical schemes for calculating the advection–diffusion equation have been developed and compared by many authors over the last 20 years, and there now exists a wide range of methods with varying degrees of accuracy and efficiency. For this study, we take our scalar evolution equation to be

$$\frac{\partial c}{\partial t} + u_i \frac{\partial c}{\partial x_i} = \frac{\partial}{\partial x_i}\left(K \frac{\partial c}{\partial x_i}\right) \qquad (1)$$

where c is the conserved scalar variable, u_i is an incompressible velocity field, and K is the diffusivity. A case of common interest in many practical situations is the advection-dominated flow, where the diffusive term on the right of Eq. (1) is small compared with the terms on the left. In this case, the numerical representation of the advective term is very important, and the ideal scheme would maintain all moments of the scalar distribution. Most finite-difference schemes manifest their failure to conserve these moments by introducing an effective numerical diffusivity, or by generating unphysical values of c. Techniques have been developed that maintain a nonnegative scalar concentration with reduced diffusivity, for example, the flux-corrected transport method of Book et al. (1975), or the schemes of Smolarkiewicz (1983) and Bott (1989). However, these methods still contain numerical diffusion whose magnitude may not be negligible compared with K.

A method based on the conservation of the first and second spatial moments of the concentration distribution was presented by Egan and Mahoney (1972, hereafter EM) and subsequently investigated by Pedersen and Prahm (1974) and Pepper and Long (1978). The method seems to have received relatively little attention, in spite of its very good conservation properties, presumably due to the additional storage required for the spatial moments. In situations where accurate conservation of the scalar and its moments is important, the extra storage can be justified, and the method becomes practical.

The moment method of Prather (1986), although apparently similar in concept, is significantly different from the EM scheme. Prather's scheme is based on computation of the moment fluxes across grid boundaries, in contrast to the redistribution of mass with moment conservation. Furthermore, there does not appear to be an obvious extension of Prather's method to include diffusive effects, while the EM scheme deals with such effects in a very natural way.

The basic method is briefly presented in the next section, with a description of the representation as a pseudo-Lagrangian collection of "puffs," which can dramatically reduce the computational storage and time for the dispersion from a localized source when the scalar only influences a relatively small number of grid boxes. The performance of the basic method in some standard tests is presented for comparison with previously tested schemes. We shall show that the basic method is inadequate, however, in the presence of certain velocity and diffusivity gradients. The extensions of the method to cover these cases are given in subsequent sections.

2. Basic method

We consider a discrete approximation to the concentration field in Eq. (1) as the sum of a number of localized functions $c^{(\alpha)}(\mathbf{x})$, each of which is zero outside a finite local region. We postpone specification of the precise form of $c^{(\alpha)}$, but we can derive exact equations for the evolution of its spatial moments from Eq. (1). We define

$$m^{(\alpha)} = \int c^{(\alpha)}(\mathbf{x}) dV$$

$$m^{(\alpha)} \bar{x}_i^{(\alpha)} = \int x_i c^{(\alpha)} dV$$

Corresponding author address: R. I. Sykes, ARAP, Division of California Research and Technology, 50 Washington Road, P.O. Box 2229, Princeton, NJ 08543.

$$m^{(\alpha)}\sigma_{ij}^{(a)} = \int [x_i - \bar{x}_i^{(\alpha)}][x_j - \bar{x}_j^{(\alpha)}]c^{(\alpha)}dV$$

where the integrals are taken over the entire distribution.

Then, from Eq. (1)

$$\frac{d}{dt} m^{(\alpha)} = 0 \tag{2}$$

and

$$\frac{d}{dt}\bar{x}_i^{(\alpha)} = \frac{1}{m^{(\alpha)}} \times \int x_i \left\{ -\frac{\partial[c^{(\alpha)}u_j]}{\partial x_j} + \frac{\partial}{\partial x_j}\left[K\frac{\partial c^{(\alpha)}}{\partial x_j}\right]\right\} dV$$

which yields, after integration by parts,

$$\frac{d}{dt}\bar{x}_i^{(\alpha)} = \frac{1}{m^{(\alpha)}}\int c^{(\alpha)}\left(u_i + \frac{\partial K}{\partial x_i}\right)dV. \tag{3}$$

Similarly, the second-moment equation can be rearranged to give

$$\frac{d}{dt}\sigma_{ij}^{(\alpha)} = \frac{1}{m^{(\alpha)}}\int c^{(\alpha)}\left(2K\delta_{ij} + x_i u_j + x_j u_i + x_i\frac{\partial K}{\partial x_j} + x_j\frac{\partial K}{\partial x_i}\right)dV \tag{4}$$

where $\mathbf{x}$ is relative to the centroid location when it appears in the integral. Thus, assuming $\mathbf{u}$ and K are constant over the range of $c^{(\alpha)}$, we obtain the well-known moment equations

$$\frac{d}{dt} m^{(\alpha)} = 0 \tag{5}$$

$$\frac{d}{dt}\bar{x}_i^{\alpha} = u_i \tag{6}$$

$$\frac{d}{dt}\sigma_{ij}^{\alpha} = 2K\delta_{ij} \tag{7}$$

expressing the conservation of mass, advection of the centroid by the local velocity, and spreading of the second moments by diffusion.

Equation (7) is solved using a simple forward time step, but the second-order-accurate Adams–Bashforth scheme is used for the centroid equation, that is,

$$\overline{x_i^{t+1}} = \overline{x_i^t} + (1.5u_i^t - 0.5u_i^{t-1})\Delta t.$$

The centroid velocity u_i is considered as a Lagrangian variable connected with each puff, that is, $u_i^t = u_i(x^t, t)$; this higher-order scheme was found to give much better conservation properties than a first-order advection scheme.

A problem with a Lagrangian puff model, particularly for a localized source, is how to maintain resolution of the small-scale structure as the puffs grow due to diffusion. Thus, after completing the advection and diffusion step, we need to "split" puffs when they exceed a certain size. However, to avoid creating too many puffs, we also want to merge puffs when they are within a certain distance of one another. Our puff splitting and merging criteria are based on fixed lengths in the x, y, and z directions. By equating these lengths with grid lengths, our method becomes nearly equivalent to that of EM.

For simplicity, we will describe a two-dimensional example, but the extension to three-dimensional puffs is straightforward. At this point we need to specify the shape of $c^{(\alpha)}$, so we take the simple "top-hat" function used by EM; that is, we consider the distribution of a scalar to be represented by many rectangular-shaped puffs with uniformly distributed mass, one of which is shown in Fig. 1. The puff is superimposed on a fixed grid designated by subscripts i and j such that grid-box centers are located at $(i\Delta x, j\Delta y)$. The puff has dimensions given by $l_x^2 = 12\sigma_{xx}$, $l_y^2 = 12\sigma_{yy}$, as defined by the second moment of a rectangular distribution; it is located at $(\bar{x}, \bar{y})$ and has mass m. The puff is split based on its overlap with neighboring grid boxes, resulting in partition parameters analogous to those of EM:

$$P_{i+1}^x = \max\left[\left(\frac{l_x}{2} + \bar{x} - x_i - \frac{\Delta x}{2}\right)l_x^{-1}, 0\right] \tag{8}$$

$$P_{i-1}^x = \max\left[\left(\frac{l_x}{2} - \bar{x} + x_i - \frac{\Delta x}{2}\right)l_x^{-1}, 0\right] \tag{9}$$

$$P_i^x = 1 - P_{i+1}^x - P_{i-1}^x. \tag{10}$$

Similar factors are computed for redistribution in the y direction. The centroid positions for the overlap regions are defined by

$$\tilde{x}_{i+1} = x_i + \Delta x/2 + P_{i+1}^x l_x/2 \tag{11}$$

$$\tilde{x}_{i-1} = x_i - \Delta x/2 - P_{i-1}^x l_x/2 \tag{12}$$

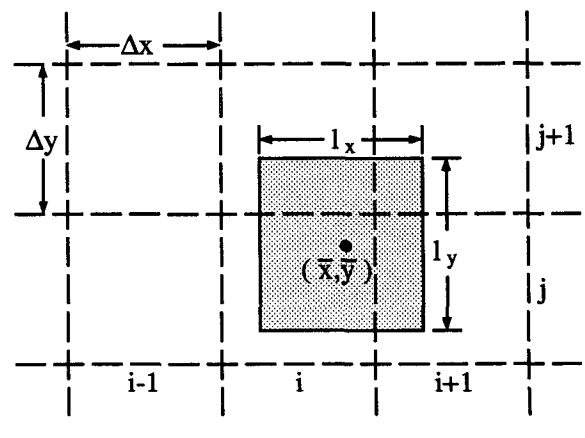

FIG. 1. Schematic illustration of a rectangular puff located on a fixed grid. In this example the puff will be partitioned into four new puffs defined by its overlap of the grid cells.

$$\tilde{x}_i = \frac{(\bar{x} - P^x_{i-1}\tilde{x}_{i-1} - P^x_{i+1}\tilde{x}_{i+1})}{P_i^x} \quad (13)$$

with similar expressions for the y direction.

The moments of the newly created puff, denoted by a subscript n, in grid box $i + \alpha, j + \beta$, where $\alpha \in \{1, 0, -1\}$ and $\beta \in \{1, 0, -1\}$ are described as follows:

$$m_n = P^x_{i+\alpha}P^y_{j+\beta}m \quad (14)$$

$$\bar{x}_n = \tilde{x}_{i+\alpha}, \quad \bar{y}_n = \tilde{y}_{j+\beta} \quad (15a,b)$$

$$\sigma_{xx_n} = \frac{(P^x_{i+\alpha}l_x)^2}{12}, \quad \sigma_{yy_n} = \frac{(P^y_{j+\beta}l_y)^2}{12} \quad (16a,b)$$

for

$$P^x_{i+\alpha} \neq 0, \quad P^y_{j+\beta} \neq 0.$$

Puffs with centroids in the same grid box are then merged to conserve mass and first and second moments. The time-lagged centroid velocity, required for the Adams–Bashforth scheme, of the merged puff is obtained from the mass-weighted mean of the velocities from the contributing puffs. In this way, the Lagrangian nature of the centroid time derivative is maintained as puffs are redistributed on the grid.

The Lagrangian nature of our scheme is essential in reducing storage requirements, since it allows us to avoid storing information (and performing computations) for grid cells with zero concentration, in contrast to fixed grid methods. However, it is apparent in the plume edges many puffs of very small concentration will be created by diffusive splitting. Assuming that the regions of small concentration do not need to be highly resolved, we set a minimum mass below which puffs are not permitted to split. They continue to diffuse and advect and may merge with other puffs. The choice of this parameter is problem dependent. We typically choose a value about four orders of magnitude smaller than the maximum expected mass. At this level, only regions with very small concentrations are poorly resolved.

3. Numerical advection test results

We shall first present some of the standard numerical advection tests with $K = 0$ for the second-moment method. The method does not seem to have been extensively tested in the literature, so these basic performance measures are necessary before discussing the improvements. Linear analysis of the method is very difficult, and we, therefore, present the advection of a one-dimensional unit sinusoidal distribution as a prototype problem; the sinusoid has a mean offset of 50 to minimize the nonlinearities associated with zero concentrations. Figure 2 shows the results for a 4Δ and an 8Δ wave traveling in the x direction at Courant numbers C of 0.25, 0.50, and 0.75; Δ is the numerical grid length. The model results are compared with the

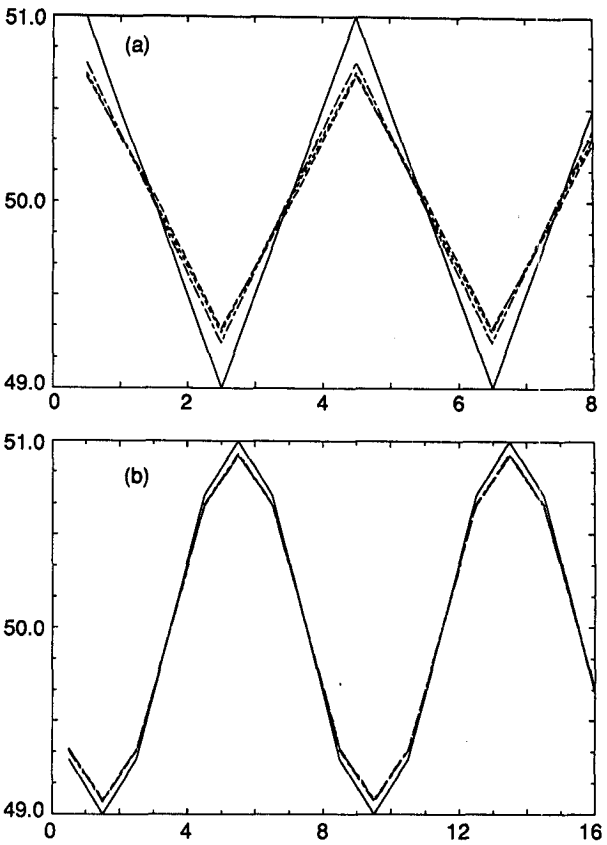

FIG. 2. Second-moment advection scheme performance for the sinusoidal wave: (a) 4Δ wavelength and (b) is 8Δ, —— exact solution; — · — $C = 0.75$; --- $C = 0.5$;— — $C = 0.25$.

analytically translated solution after a time period of $3/C$. These results can be compared directly with those of Smolarkiewicz and Clark (1986) and also Bott (1989). The second-moment method shows very small phase errors and very little sensitivity to Courant number. The 4Δ wave results also show very good conservation properties, even in comparison with the fourth-order scheme of Bott (1989), while the 8Δ wave results are more comparable with the second-order scheme.

Another standard numerical advection test is the rotating flow field, which has been used to evaluate the second-moment method by Chock and Dunker (1983). They indicated the importance of the accuracy of the trajectory calculation for the centroid and showed results using an exact computation of the centroid displacement and also a simple first-order, forward time-step prediction. Our results use the second-order Adams–Bashforth time discretization, which gives a much improved prediction of the trajectory. The results for the 4Δ radius cosine hill centered at a distance of 10Δ from the center of a 33 × 33 grid, that is, the same as computed by Chock and Dunker, for time steps of 15π and 60π are given in Table 1. The time steps imply

TABLE 1. Results for the solid-body rotation of a cosine hill on the 33 × 33 grid after two rotations. Errors are specified relative to the initial hill height of 100.

Method	Δt	$\Sigma c^2/\Sigma c_0^2$	E_{max}	E_{avg}	CPU (s)
Present	15π	0.92	22	0.21	22
Present	60π	0.90	24	0.25	5
Egan and Mahoney	15π	0.78	38	0.6	190
SHASTA	15π	0.3	75	1.4	44
Prather	15π	0.97	2	0.06	102
Prather	60π	0.96	2	0.05	26

480 and 120 steps per revolution, respectively, and the results are presented after two complete revolutions. The results are obviously much better than those obtained by Chock and Dunker for the second-moment method of Egan and Mahoney, which we attribute to the improved accuracy of the centroid displacement calculation, and again show little sensitivity to Courant number. The present results are superior to those from any of the positive-definite schemes tested by Chock and Dunker. Results of the flux-correction scheme SHASTA, as presented in Chock and Dunker (1983) and Prather (1986) are also included. The present-moment method is clearly superior to SHASTA, but not as accurate as Prather's scheme, although the execution times do seem significantly smaller. The CPU times are estimated assuming that a single processor on the Silicon Graphics 4D/240 is 15 times faster than a VAX 11/780. The faster execution times for our code result from the Lagrangian nature of the calculation, which only requires about 80 puffs to represent the cosine hill; all other cells are empty and are not represented in the calculation at all.

A more highly resolved linear cone, with radius 15Δ and center at 25Δ from the center of a 100×100 grid, has also been used by researchers. The results after six revolutions (3768 steps) are given in Table 2 and compared with several other schemes; the actual result from the second-moment calculation is shown in Fig. 3. The conservation properties compare favorably with the fourth-order scheme of Bott (1989), but the moment-conservation scheme of Prather (1986) maintains the peak value more accurately. The integral moment, however, is conserved very accurately by our method, and the linear cone shows very little distortion under advection by the scheme.

TABLE 2. Results for the solid-body rotation of a conical hill on the 100 × 100 grid after six rotations.

Method	$\Sigma c^2/\Sigma c_0^2$	C_{max}/C_0
Present	0.995	0.87
Smolarkiewicz	0.87	0.84
Bott $l = 2$	0.919	0.82
Bott $l = 4$	0.966	0.86
Prather	0.998	0.99

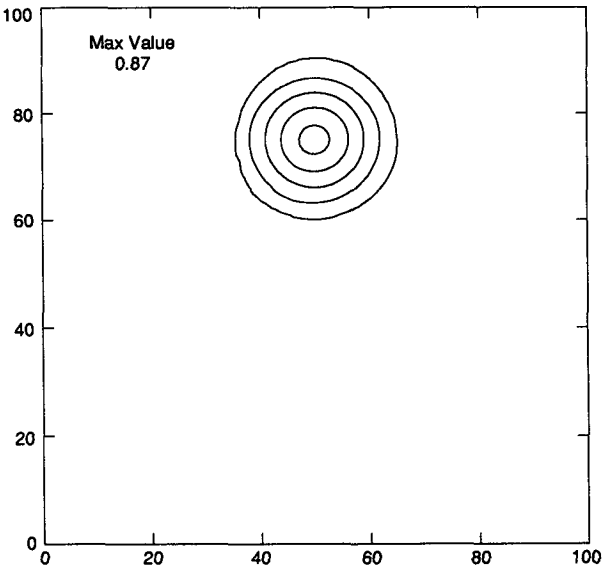

FIG. 3. Second-moment advection scheme result for the conical hill transport after six revolutions on a 100 × 100 grid. Contours are at 0.02, 0.2, 0.4, 0.6, and 0.8 relative to a unit initial height.

The deformational flow field introduced by Smolarkiewicz (1982) has also been used as a numerical advection test flow. In this flow,

$$u = \frac{8\pi}{25} \sin\left(\frac{\pi x}{25}\right) \sin\left(\frac{\pi y}{25}\right)$$

$$v = \frac{8\pi}{25} \cos\left(\frac{\pi x}{25}\right) \cos\left(\frac{\pi y}{25}\right)$$

and the advection of an initially conical distribution centered on the origin has been examined by Smolarkiewicz (1982) and Bott (1989).

Using the same numerical parameters as previous investigators, the basic scheme discussed in the preceding tests shows some problem with this flow, as can be seen from Fig. 4. The solution after 75 steps shows several "spikes," which are associated with the stagnation points in the flow. Away from these points, the solution is generally good. The solution spikes are due to the flux imbalances across grid boundaries, which result from the use of centroid velocities in a nonuniform flow field. The problem can be dramatically reduced by the inclusion of the velocity gradient terms in the second-moment equation (7). Using a first-order Taylor series expansion to represent the velocity field in the locality of the puff, that is, $u_i = u_i(\bar{\mathbf{x}}) + x_j(\partial u_i/\partial x_j)$, an improved expression for the second-moment evolution equation can be obtained from Eq. (4). This gives (dropping the superscript α)

$$\frac{d}{dt}\sigma_{ij} = 2K\delta_{ij} + \sigma_{ik}\frac{\partial u_j}{\partial x_k} + \sigma_{jk}\frac{\partial u_i}{\partial x_k}. \qquad (17)$$

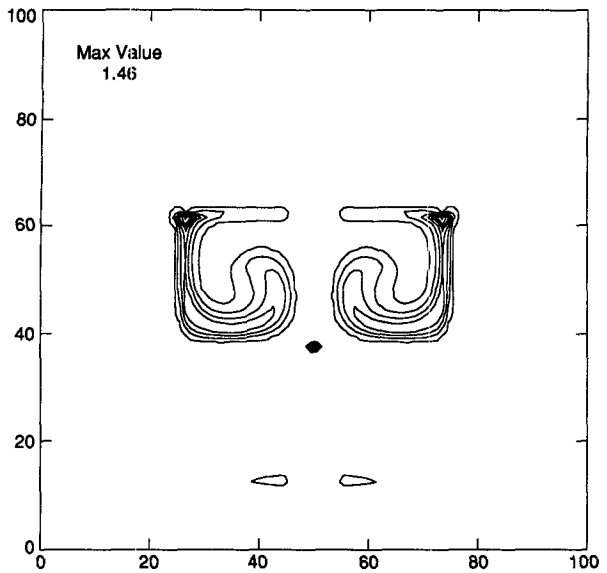

FIG. 4. Second-moment advection scheme results for the deformation flow field after 75 time steps using Eq. (7). Contours are at 0.02, 0.2, 0.4, 0.6, and 0.8.

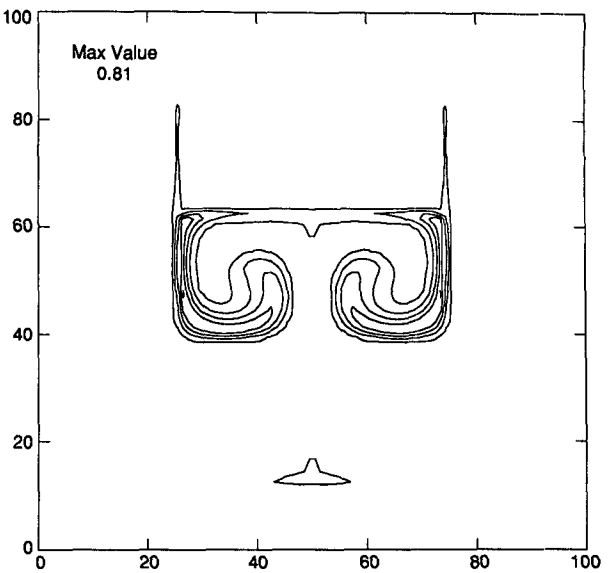

FIG. 5. Second-moment advection scheme results for the deformation flow field after 75 time steps using Eq. (17). Same contours as Fig. 4.

For the diagonal moments of our two-dimensional puff representation, Eq. (17) becomes

$$\frac{d}{dt}\sigma_{xx} = 2K + 2\sigma_{xx}\frac{\partial u}{\partial x}, \qquad \frac{d}{dt}\sigma_{yy} = 2K + 2\sigma_{yy}\frac{\partial v}{\partial y}. \tag{18a,b}$$

We employ a semianalytic approximation for the numerical solution of these equations, so that

$$\sigma_{xx}(t + \Delta t) = \sigma_{xx}(t)\exp(2\Delta t\partial u/\partial x) + 2K\Delta t \tag{19}$$

and similarly for σ_{yy}. The exponential formulation is used so that the volume (area in two-dimensional cases) of the puff is exactly conserved in the absence of diffusion.

Equation (17) is the general tensor moment equation, but we find several practical reasons for treating only the diagonal terms. The foremost of these is the fact that we are only using diagonal moments to describe the puff itself, so that off-diagonal components do not contribute. Extension of the method to include subgrid skew distributions would require much more complicated decomposition rules to reassign puff mass among the grid boxes. We, therefore, rely on explicit representation of the skewness. Second, as noted above, it is very straightforward to conserve puff volume using only diagonal moments. Finally, we find that the diagonal moments are much more important in the flux estimates.

The improvement obtained from the additional terms can be seen in Fig. 5, where it is clear that the spikes have been eliminated. The velocity-gradient tensor is diagonal at the problem points, and the new terms significantly improve the flux balance for these grid boxes. The comparison with the scheme of Bott (1989) is very good, and the method is also stable in the long-term integration. The finescale structure of

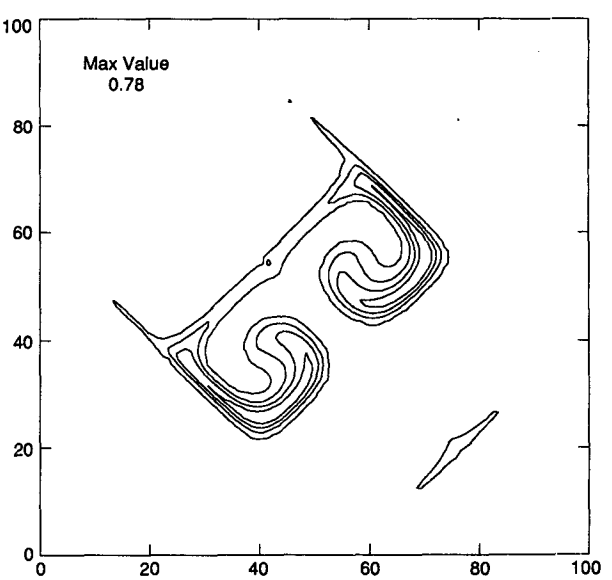

FIG. 6. Second-moment advection scheme results for the deformation flow field rotated through 45° after 75 time steps. Same contours as Fig. 4.

the late-time solution cannot be represented on the grid (Staniforth et al. 1987), but the numerical solution does produce the broad features of the analytical result.

In order to test the neglect of the off-diagonal moments, Fig. 6 is a repeat of Fig. 5 with the flow rotated through 45°. In this case, the velocity-gradient tensor is purely off-diagonal at the problem points in Fig. 4, so that the new terms added in Eq. (18) are zero, that is the model equations are identical to those used to obtain Fig. 4. The results, however, are very close to those in Fig. 5. The rotated computation shows no evidence of spikes, indicating the dominance of the diagonal moment corrections. There are differences between Figs. 5 and 6, but the maximum values are very similar, while the very narrow ridges at the sides of the distribution are probably resolved differently on the two grids. These ridges are aligned with the y axis, so that the 45° case effectively has a larger grid length by a factor of $\sqrt{2}$.

4. Nonuniform diffusivity

The use of Eq. (7) to simulate the diffusion process can result in serious errors for nonuniform diffusivity. As examples, we show results for linear and parabolic diffusivity profiles. A single puff is released into a zero wind field bounded by walls at $z = \pm L$ after which it starts to diffuse. We limit the diffusion to the vertical direction so that this is a one-dimensional problem and the steady-state concentration should be uniform.

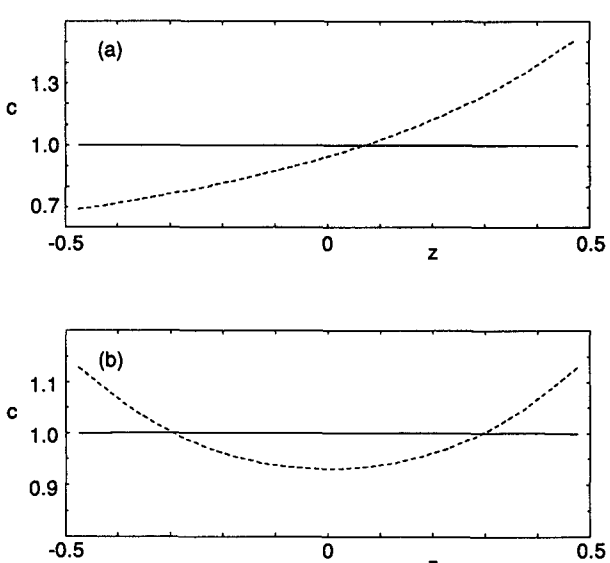

FIG. 7. Concentration profiles for the one-dimensional diffusion tests. Dashed lines are the results using Eq. (7) and solid lines are results from Eq. (22). (a) Linear diffusivity profile given by Eq. (20) and (b) parabolic profile given by Eq. (21).

Figures 7a,b show the solutions for the linear and parabolic diffusivity profiles, respectively (dashed lines), and they are notably nonuniform. Here the linear diffusivity profile is given by

$$K = K_o(1 - \xi z/L) \tag{20}$$

and the parabolic profile is given by

$$K = K_o[1 - \xi(z/L)^2] \tag{21}$$

where $K_o = 2$ and $\xi = 0.8$. The grid spacing was 0.05 with $L = 0.5$.

In a similar manner to the velocity gradient, the solution to this problem is the consideration of the diffusivity gradient, which introduces a "diffusion velocity," so that the centroid equation becomes

$$\frac{d}{dt}\bar{x}_i = u_i + \frac{\partial K}{\partial x_i}. \tag{22}$$

The solid lines in Figs. 7a,b are the solutions with this term included and are nearly constant. The linear profile case has a maximum error of 0.1% while the parabolic case has a maximum error of 0.2%. We note that this is a trivial problem for Eulerian diffusion calculations and is a source of difficulty only for a Lagrangian solution. The use of Eq. (22) is necessary for the second-moment scheme and allows accurate solutions to be computed.

5. Conclusion

We have shown how the moment method of Egan and Mahoney (1972) can be implemented as a Lagrangian puff scheme for the advection–diffusion equation, resulting in a potentially great reduction in storage requirements. The application of this scheme is best suited to a situation where the scalar quantity of interest exists in a relatively small region compared to the region of background meteorology, for example, a small source release of a pollutant.

The basic scheme has been tested with the standard solid-body-rotation velocity field, showing excellent results, in part due to the implementation of the Adams–Bashforth method for advection. It is shown that inhomogeneities of the velocity and diffusivity fields are not handled adequately by the basic method. By taking into account velocity and diffusivity gradients, results are dramatically improved.

The improvements to the method are not particularly time consuming and can be important, particularly near boundaries. For example, we have found that the velocity and diffusivity gradients near the ground can be significant in a calculation of concentration means and fluctuations due to a small source release in a turbulent boundary layer.

Acknowledgements. This work was supported by the Electric Power Research Institute.

REFERENCES

Book, D. L., J. P. Boris, and K. Hain, 1975: Flux-corrected transport II: Generalization of the method. *J. Comp. Phys.*, **18,** 248–243.

Bott, A., 1989: A positive definite advection scheme obtained by nonlinear renormalization of the advective fluxes. *Mon. Wea. Rev.*, **117,** 1006–1015.

Chock, D. P., and A. M. Dunker, 1983: A comparison of numerical methods for solving the advection equation. *Atmos. Env.*, **17,** 11–24.

Egan, B. A., and J. R. Mahoney, 1972: Numerical modeling of advection and diffusion of urban area source pollutants. *J. Appl. Meteor.*, **11,** 312–322.

Pedersen, L. B., and L. P. Prahm, 1974: A method for numerical solution of the advection equation. *Tellus,* **26,** 594–602.

Pepper, D. W., and P. E. Long, 1978: A comparison of results using second-order moments with and without width correction to solve the advection equation. *J. Appl. Meteor.*, **17,** 228–233.

Prather, M. J., 1986: Numerical advection by conservation of second-order moments. *J. Geophys. Res.*, **91,** 6671–6681.

Smolarkiewicz, P. K., 1982: The multidimensional Crowley advection scheme. *Mon. Wea. Rev.*, **110,** 1968–1983.

——, 1983: A simple positive definite advection scheme with small implicit diffusion. *Mon. Wea. Rev.*, **111,** 479–486.

——, and T. L. Clark, 1986: The multidimensional positive definite advection transport algorithm: Further development and applications. *J. Comp. Phys.*, **67,** 396–438.

Staniforth, A., J. Côte, and J. Pudykiewicz, 1987: Comments on "Smolarkiewicz's deformational flow." *Mon. Wea. Rev.*, **115,** 894–900.